Pulsating flow maldistribution within an axisymmetric catalytic converter-flow rig experiment and transient CFD simulation

Liu, Z. , Benjamin, S.F. and Roberts, C.A.

SAE TECHNICAL PAPER SERIES

2003-01-3070

Pulsating Flow Maldistribution within an Axisymmetric Catalytic Converter - Flow Rig Experiment and Transient CFD Simulation

Z. Liu, S. F. Benjamin and C. A. Roberts
Coventry University

Reprinted From: Emissions: Advanced Catalyst and Substrates, Measurement and Testing, and Diesel Gaseous Emissions (SP–1801)

Powertrain & Fluid Systems Conference & Exhibition
Pittsburgh, Pennsylvania USA
October 27-30, 2003

SAE International™

400 Commonwealth Drive, Warrendale, PA 15096-0001 U.S.A. Tel: (724) 776-4841 Fax: (724) 776-5760 Web: www.sae.org

ISBN 0-7680-1319-4

Printed in USA

2003-01-3070

Pulsating Flow Maldistribution within an Axisymmetric Catalytic Converter - Flow Rig Experiment and Transient CFD Simulation

Z. Liu, S. F. Benjamin and C. A. Roberts
Coventry University

ABSTRACT

This paper investigates the flow maldistribution across the monolith of an axisymmetric catalyst assembly fitted to a pulsating flow test rig. Approximately sinusoidal inlet pulse shapes with relatively low peak/mean ratio were applied to the assembly with different amplitudes and frequencies. The inlet and outlet velocities were measured using Hot Wire Anemometry. Experimental results were compared with a previous study, which used inlet pulse shapes with relatively high peak/mean ratios. It is shown that (i) the flow is more maldistributed with increase in mass flow rate, (ii) the flow is in general more uniformly distributed with increase in pulsation frequency, and (iii) the degree of flow maldistribution is largely influenced by the different inlet velocity pulse shapes. Transient CFD simulations were also performed for the inlet pulse shapes used in both studies and simulations were compared with the experimental data. For inlet pulse shapes with low peak/mean ratio, CFD predictions matched measurements fairly well in the bulk central region of the monolith. For inlet pulse shapes with high peak/mean ratio, agreement was less satisfactory. This is probably due to the inaccuracy of the Reynolds Averaged Navier Stokes (RANS) k-ε turbulence model under such conditions.

INTRODUCTION

Flow maldistributon within the catalytic converter has been the subject of much research ever since the autocatalyst was first introduced in the 1970's. Maldistributed flow affects catalyst warm-up, light-off, conversion efficiency, pressure drop, overall utilisation efficiency and life time [1-4]. Extensive experimental and theoretical investigations have been performed to characterise the flow distribution. Early studies were performed for steady flow conditions [5,6]. However in production systems the scavenging process of the reciprocating engine generates strong exhaust pulsations, with both Under-Body Catalysts (UBC) and Close-Coupled Catalysts (CCC) being subjected to pulsating flow regimes.

Experimental studies of the flow field in autocatalysts have been reported with firing and motored engines [7-10]. The exhaust pulse shape in a real engine environment usually features a dominant 'blow-down' peak, with secondary peaks caused by 'piston displacement' and pressure harmonics in the exhaust system. The pulse shapes are very complex and it is difficult to establish their influence on flow maldistribution. Flow rigs with mechanical pulse generators are often used as they provide more clearly defined pulse shapes [11-13]. Sinusoidal shape pulses have been used in previous studies to represent the 'blow-down' dominated engine exhausts [7,18,21].

Over the past decade or so Computational Fluid Dynamics (CFD) has been widely used in the automotive industry to simulate the flow within the converter. Steady flow CFD models were used in some studies [5,6,15] as they are much less demanding of computational resources compared to transient models. With the rapid enhancement of hardware, large transient CFD models have recently been reported [14,16,17]. CFD simulations have become increasingly important for aftertreatment system design in contrast to time-consuming and costly experimental programmes. However their accuracy needs confirming before they can be used with confidence. Hence experimental validation is still necessary. To date most CFD studies on catalytic converters have only been qualitatively compared with experiment. Few systematic quantitative comparisons between CFD and measurement are reported for the particular case of flow maldistribution in a catalytic converter under pulsating flow conditions.

In this study an isothermal pulsating flow rig, fitted with an axisymmetric catalyst assembly, was utilised to represent a typical UBC configuration. Approximately sinusoidal pulses with relatively low peak/mean ratio were input to the converter. The Hot Wire Anemometry (HWA) technique was used to measure the inlet and outlet velocities of the catalyst assembly. Measurements were compared with the findings in a previous study [21], which used inlet pulse shapes with relatively high peak/mean ratios. The effect of mass flow rate and pulsation frequency on the flow distribution was studied.

For both inlet pulse shapes, transient CFD simulations were performed and predictions of the velocity downstream of the monolith were compared with measurements.

FLOW RIG EXPERIMENT

EXPERIMENTAL APPARATUS AND OPERATION

The pulsating flow rig has been previously described in detail [18,21]. A schematic of the working section is shown in figure 1. The air is fed into the pulse generator uniformly from a converging nozzle (not shown in figure 1) at room temperature. The rotating plate in the pulse generator causes asymmetric inlet flows when the pulsation frequency is high. Therefore a flow straightener is placed immediately downstream of the pulse generator to minimise the flow asymmetry. Housed in the flow straightener are double unwashcoated 400 CPSI ceramic substrates, which redistribute the flow more uniformly prior to entering the inlet pipe. A hot wire probe can be inserted into the inlet pipe through a chuck in order to monitor the inlet velocity, the probe axis being perpendicular to the flow direction. The inlet pipe has an internal diameter of 48 mm, on which all Reynolds numbers are based. A 60 mm long 60^o total angle diffuser is placed between the inlet pipe and the cylindrical substrate monolith. The 400 CPSI unwashcoated ceramic monolith has a diameter of 118 mm and length of 152 mm. A 50 mm long outlet pipe is placed downstream of the monolith in order to avoid entrainment of surrounding air when measuring outlet velocities. The rig is bench mounted horizontally as in figure 1 and the outlet velocity profiles are measured along the horizontal (x) and vertical (y) axis in a circular plane 30 mm downstream of the monolith exit (hereinafter called the 'measurement plane'). This is to avoid the individual channel jets when the flow leaves the monolith [4].

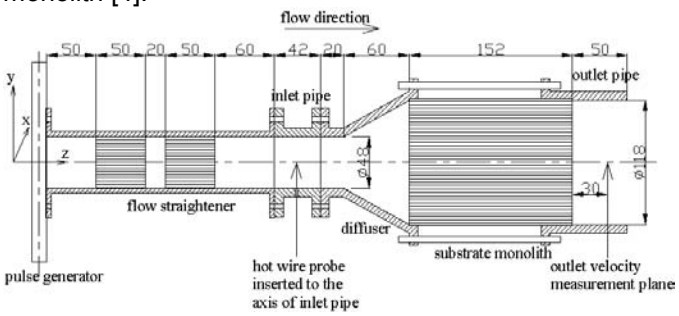

Figure 1 - Schematic of the flow rig

When measuring the outlet velocity, the probe axis is parallel with the flow direction. The probe is attached to an automatic 2D traverse, which significantly improves positioning accuracy and enables fast velocity profiling. An IFA 300 constant temperature HWA system from TSI inc. was used in this study. A 1 MHz 4 channel 12 bit A/D converter was used to convert the IFA 300 output voltage (within ± 5 V) to a digital signal, which is then processed by the TSI ThermalPro software. The instantaneous and time averaged velocity, as well as the velocity profile, can be obtained by the ThermalPro software.

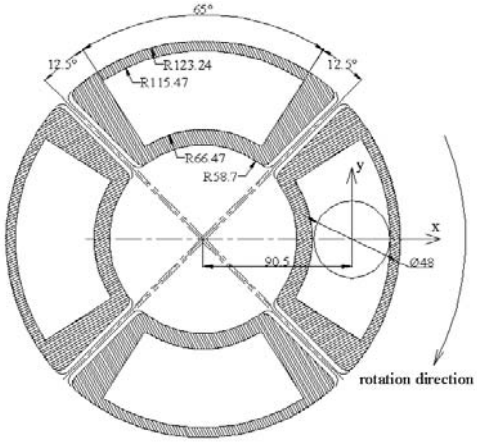

Figure 2 - Schematic of the pulse generator inserts (viewed from right to left in figure 1)

The pulse generator contains a cast iron rotor plate in an aluminium housing. Four inserts are evenly spaced around the plate. The rotor plate is driven by a DC motor. Different hole shapes can be designed for the pulse generator inserts to readily change velocity pulse shapes when the rotating plate intermittently opens and closes the flow path. A schematic of the four inserts used in this study is shown in figure 2. The open and blocked section per insert is 65^o and 25^o respectively. As an approximately 30^o blank section is needed to fully block the 48 mm diameter flow passage, the current insert geometry ensures that the pulse generator is never fully closed at any time instant. An optical-electrical transducer (± 5 V output voltage) is embedded in the pulse generator housing. The output voltage of the transducer is connected to the A/D board and hence can be read by the ThermalPro software. This serves both as a rotation frequency counter and as a timing signal for velocity measurements. Utilising this timing signal, the measured velocities were ensemble averaged over at least 25 cycles to minimise cycle-to-cycle variation. The hot wire probes used are 55P11 type single cylindrical sensors from DANTEC, 5 µm in diameter and 1.25 mm long. A Model 1129 air velocity calibrator from TSI was used to calibrate the wires.

The actual mass flow rate for each flow condition was calculated by integrating the outlet velocity profiles in the measurement plane and it covers a wide range from ~7000 Re to ~73000 Re. The inlet velocity for pulsating flows is measured by inserting a hot wire probe into the inlet pipe, as shown in figure 1. The actual frequency for each flow condition was calculated using the ensemble averaged inlet velocity at the centre of the inlet pipe. The frequencies used in this study are 0 Hz (steady state) and ~15, 31, 49, 63, 78, 98 Hz.

INLET VELOCITY PULSE SHAPES

With the flow straightener added between the pulse generator and the inlet pipe, the inlet velocity is fairly spatially uniform. Figure 3 shows the inlet velocities at the centre of the inlet pipe at ~31 Hz for different mass flow rates. Figure 4 shows the inlet velocities with ~70000 Re for different frequencies. All inlet velocities

shown in both figures are ensemble averaged and repeated for four cycles. They are also the prescribed inlet velocities for the transient CFD models discussed later. The pulses in general approximate to sinusoidal shapes. For the lower frequency (< ~50Hz) cases in figures 3 and 4, smooth pulses were produced. However with an increase in pulsation frequency, relatively stronger velocity fluctuations were observed and the pulses were less regular in shape (figure 4 d-f). This may be due to pressure wave harmonics within the catalyst assembly at these frequencies.

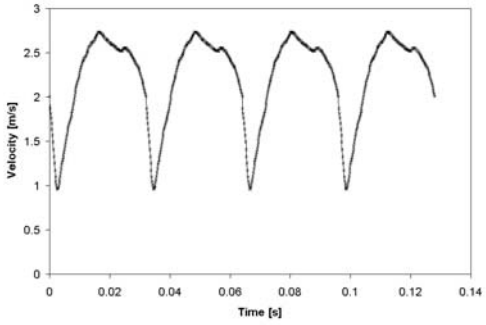

(a) Re = ~7000, Frequency = ~31 Hz

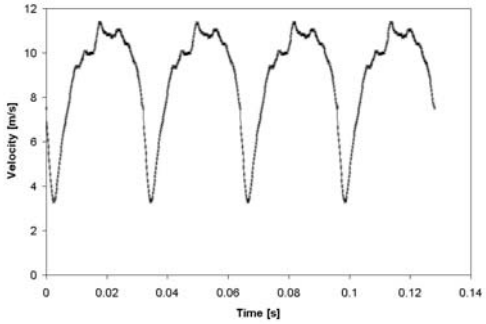

(b) Re = ~29000, Frequency = ~31 Hz

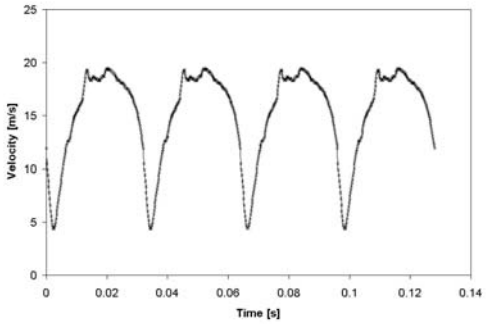

(c) Re = ~48000, Frequency = ~31 Hz

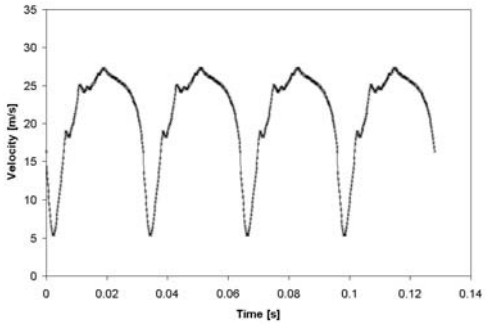

(d) Re = ~67000, Frequency = ~31 Hz

Figure 3 - inlet velocities at ~31 Hz for different mass flow rates

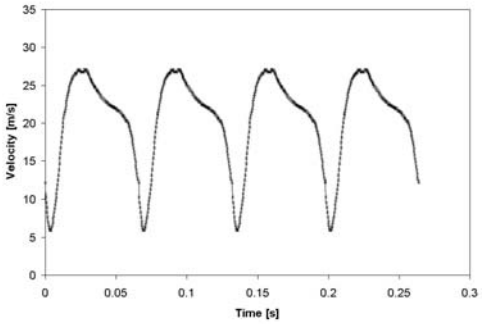

(a) Re = ~65000, Frequency = ~15 Hz

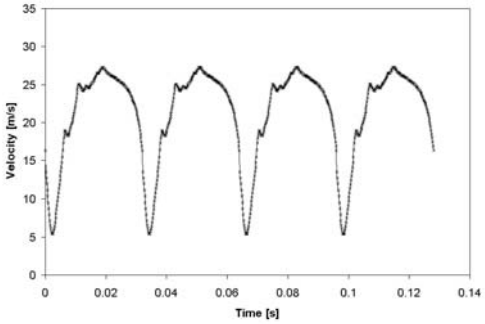

(b) Re = ~67000, Frequency = ~31 Hz

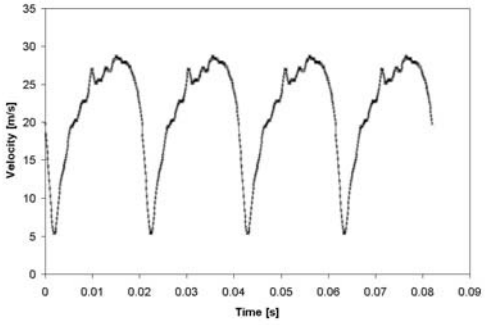

(c) Re = ~70000, Frequency = ~49 Hz

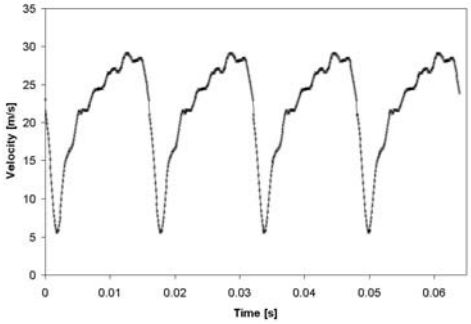

(d) Re = ~70000, Frequency = ~63 Hz

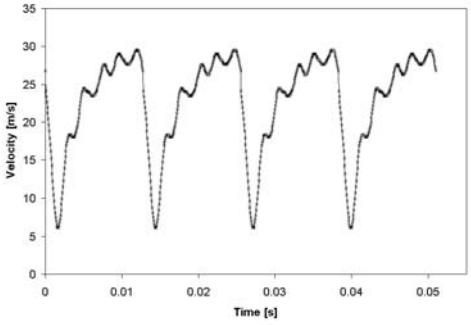

(e) Re = ~72000, Frequency = ~78 Hz

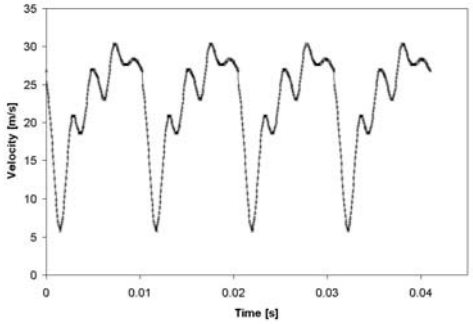

(f) Re = ~72000, Frequency = ~98 Hz

Figure 4 - inlet velocities with ~70000 Re for different frequencies

EXPERIMENTAL RESULTS

The effect of mass flow rate on the flow distribution

To study the effect of different mass flow rates on the flow distribution, the cycle-averaged outlet velocity profiles along the horizontal (x) and vertical (y) axis in the measurement plane (see figure 1) were compared as in figure 5 for ~31 Hz pulsation frequency with different mass flow rates (from ~7000 Re to ~67000 Re). For a fixed pulsation frequency (e.g. ~31 Hz for this case) the flow is more maldistributed with the increase in mass flow rate. When the inlet velocity is low, the flow is relatively attached to the diffuser wall. With an increase in mass flow rate, the flow separates and recirculates in the diffuser, causing a jet in the central region of the monolith and hence more maldistributed flow. The result is consistent with a previous experimental study [21].

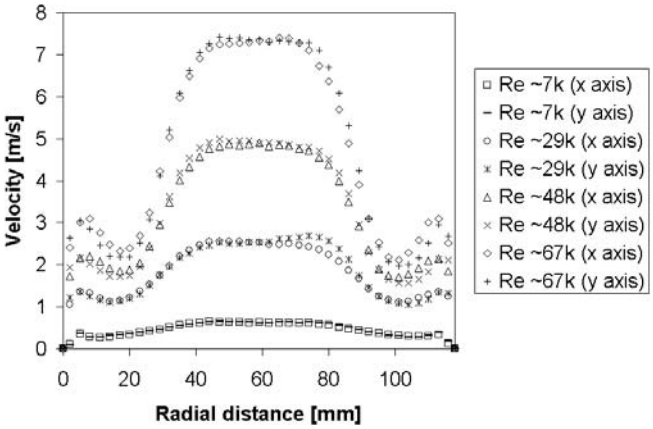

Figure 5 - Cycle-averaged outlet velocity profiles at ~31 Hz for different mass flow rates

The effect of pulsation frequency on the flow distribution

To study the effect of pulsation frequency on the flow distribution, the cycle-averaged outlet velocity profiles with ~70000 Re for different frequencies are shown in figure 6. Since the actual Reynolds number was slightly different from case to case, the outlet velocities are normalised.

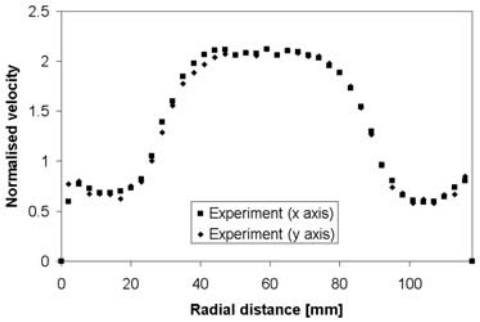

(a) Re = ~73000, steady state

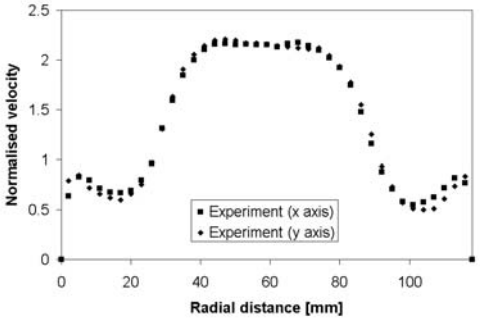

(b) Re = ~65000, Frequency = ~15 Hz

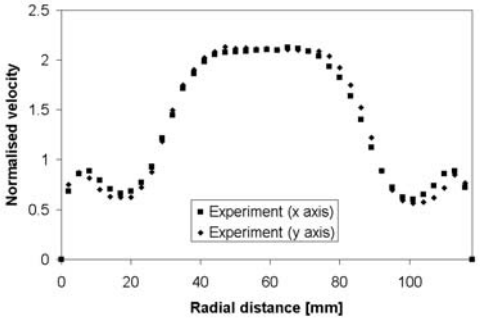

(c) Re = ~67000, Frequency = ~31 Hz

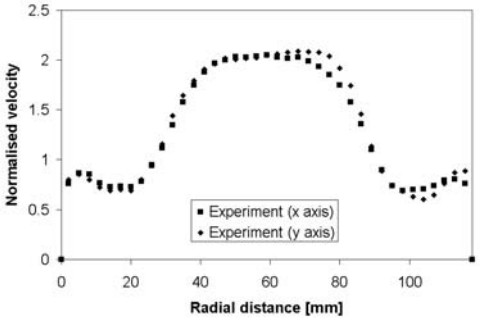

(d) Re = ~70000, Frequency = ~49 Hz

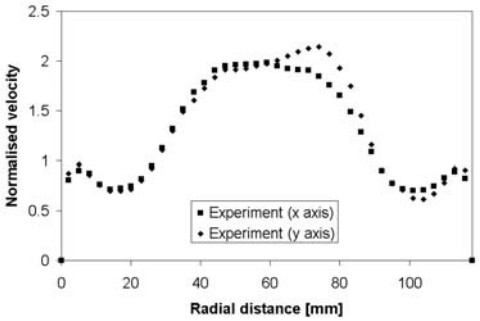

(e) Re = ~70000, Frequency = ~63 Hz

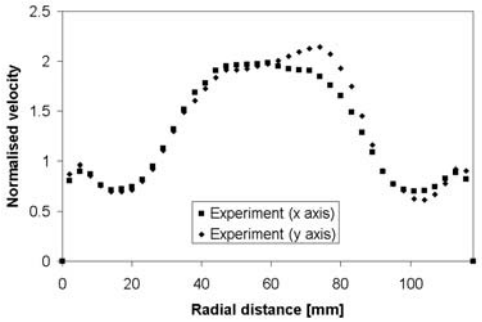

(f) Re = ~72000, Frequency = ~78 Hz

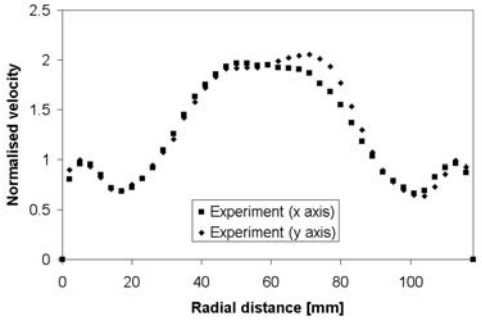

(g) Re = ~72000, Frequency = ~98 Hz

Figure 6 - Cycle-averaged outlet velocity profiles for steady and pulsating flows with ~70000 Re

To quantitatively illustrate the relationship between pulsation frequency and flow maldistribution, a non-uniformity index was defined. The non-uniformity index utilises the mass flow weighted velocity integrated over the substrate face. The variation of the velocity, σ_V, is defined according to equation 1.

$$\sigma_V = \frac{1}{\dot{m}} \int_S \left| V_i - \bar{V} \right| \cdot \delta \dot{m} \qquad (1)$$

where $\dot{m}$ is the mass flow rate, V_i is the individual channel velocity, $\bar{V}$ is the mean velocity across the monolith obtained from equation 2 and S is the cross sectional area of the monolith.

$$\bar{V} = \frac{1}{\dot{m}} \int_S V_i \cdot \delta \dot{m} \qquad (2)$$

The non-uniformity index Λ over the cross section of the substrate is calculated according to equation 3.

$$\Lambda = \frac{\sigma_V}{\bar{V}} \times 100 \qquad (3)$$

A non-uniformity index of zero means that the flow distribution is perfectly uniform across the substrate. The larger the non-uniformity index, the more maldistributed the flow.

Figure 7 compares the non-uniformity indices at ~70000 Reynolds number between this study and a previous study [21], which used the same flow rig but produced inlet pulse shapes with higher peak/mean ratios. The index values for both studies were taken as the average indices of the x and y axes. Figure 8 compares the ensemble averaged inlet velocities for both studies.

Both studies indicate that in general the flow across the catalyst monolith becomes less maldistributed as pulsation frequency increases. The reasons for this are possibly two fold. Firstly, at low frequencies the flow has relatively more time to establish the inertia dominated steady flow characteristics of flow separation and recirculation in the diffuser, leading to maldistributed flow at high Reynolds number. With an increase in frequency, the flow has less time to develop the inertia effect hence the distribution becomes more uniform. Secondly, at high frequencies it is more likely that more than one pulse resides in the diffuser volume at any time instant, leading to pulse interaction and hence increased mixing.

Figure 7 also shows that the flow is more maldistributed in this study than observed previously in [21] at the same frequency. The reasons for this are believed to be due to the difference between the inlet pulse shapes used in the two studies. Firstly, the pulse generator used in [21] had some 'fully-closed' periods as shown in figure 8, whilst in this study it was never completely closed. The inlet pulses in [21] may thus resemble discrete 'puffs' rather than the continuous jets generated in this study. This will lead, in the former case, to more mixing and hence flatter velocity profiles. Secondly, the greater acceleration/deceleration of the inlet pulses in [21] will cause stronger shear between the central jet and the surrounding fluid in the recirculation zone within the diffuser, resulting in more uniform flow distributions.

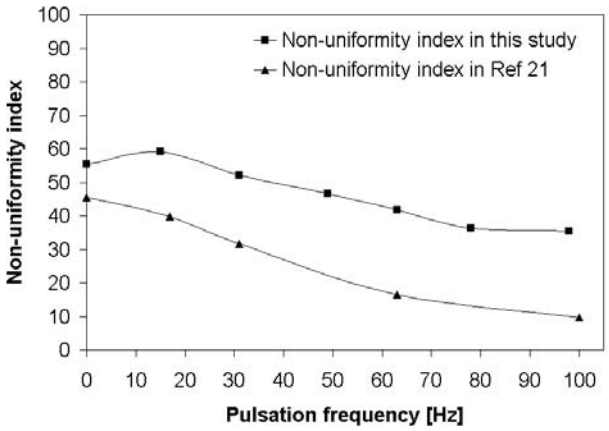

Figure 7 - Comparisons of the non-uniformity index

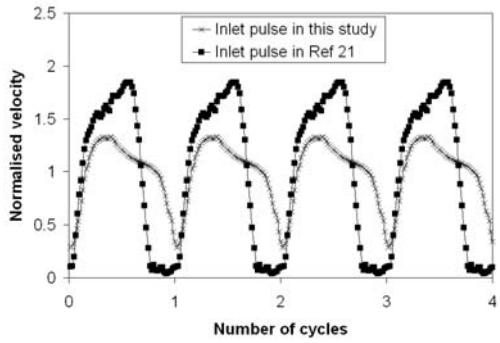

Inlet pulse in this study:
Re= ~ 65000, frequency = ~ 15 Hz, peak/mean = 1.32
Inlet pulse in Ref 21:
Re = ~ 57000, frequency = ~ 17 Hz, peak/mean = 1.84

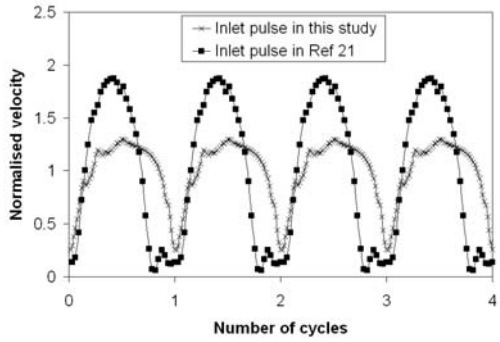

Inlet pulse in this study:
Re= ~ 67000, frequency = ~ 31 Hz, peak/mean = 1.30
Inlet pulse in Ref 21:
Re = ~ 72000, frequency = ~ 31 Hz, peak/mean = 1.87

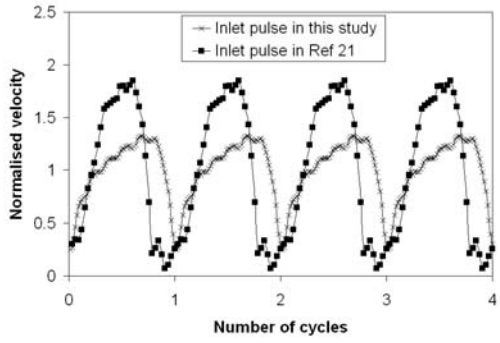

Inlet pulse in this study:
Re= ~ 70000, frequency = ~ 63 Hz, peak/mean = 1.32
Inlet pulse in Ref 21:
Re = ~ 66000, frequency = ~ 63 Hz, peak/mean = 1.85

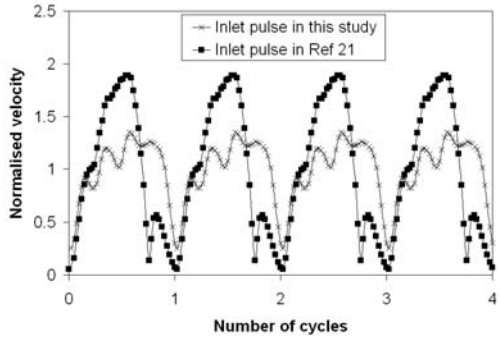

Inlet pulse in this study:
Re= ~ 72000, frequency = ~ 98 Hz, peak/mean = 1.35
Inlet pulse in Ref 21:
Re = ~ 73000, frequency = ~ 100 Hz, peak/mean = 1.89

Figure 8 - Comparisons of inlet pulse shapes

CFD MODELLING OF THE CATALYST ASSEMBLY

MESH GENERATON

A general purpose commercial CFD code, STAR-CD [19], was used to simulate the flow in the catalyst assembly. Since the geometry is axisymmetric, only a 5 degree wedge section was modelled. As shown by figure 9 a multi-block approach was used to set up the mesh for application of the 'two-layer' turbulence model, with the X, Y, Z axes being the radial, circumferential and axial directions respectively. The mesh comprises 10 blocks of cells. A 96mm long inlet tube (blocks 1, 2, 6 and 7) leads into a conical diffuser (blocks 3 and 8). The substrate monolith (blocks 4 and 9) is located downstream of the diffuser followed by a 30mm long outlet sleeve (blocks 5 and 10). The mesh has 28314 cells in total and comprises 363 axial cells and 78 radial cells, of which 58 cells are for the high Reynolds number region (blocks 1-5) and 20 are for the 9 mm near wall region (blocks 6-10). A higher axial density of cells was used in the diffuser (blocks 3 and 8) and the short inlet section (blocks 2 and 7) immediately upstream to ensure that flow separation, recirculation and reattachment in the diffuser can be captured by the calculation. A mesh independence study was reported in [22], which shows that the current grid resolution is sufficient.

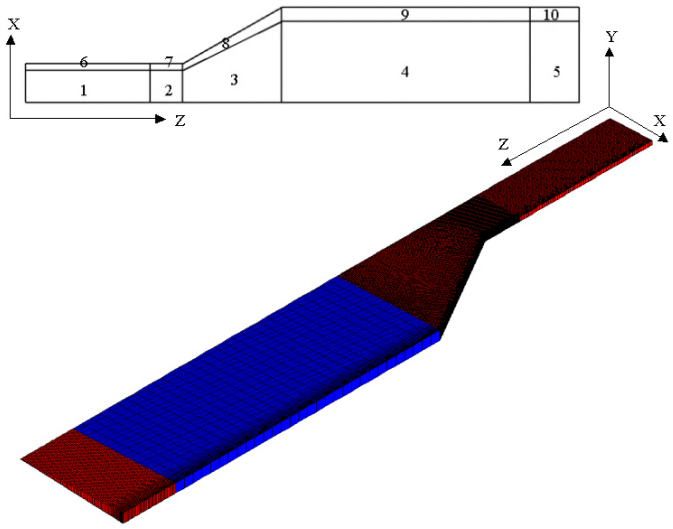

Figure 9 - CFD mesh structure

The two side faces of the wedge were defined as 'symmetry planes'. The inlet plane of was defined as an 'inlet boundary' with a uniform axial velocity corresponding to the Reynolds numbers recorded in the experiments. The exit plane was defined as a 'pressure boundary'. The RANS quadratic non-linear k-ε model was selected in the high Reynolds number region and the Norris & Reynolds one equation model was used for the near-wall treatment [19].

POROUS MEDIUM APPROACH

A typical automotive catalyst monolith is comprised of several thousand small channels and resolving the flow details within every channel would require prohibitively large computing resources. A widely adopted alternative approach is to treat the monolith as an equivalent continuum or porous medium with special properties [10, 13].

The porous medium is described as a distributed flow resistance, where assuming a local balance between the pressure and resistance forces such that

$$\frac{\Delta p}{L} = (\alpha|\boldsymbol{v}| + \beta)u \qquad (4)$$

where $\Delta p / L$ is the pressure loss per unit length, u is the superficial velocity in one of the three orthogonal directions, α and β are user-supplied permeability coefficients in that direction and $|\boldsymbol{v}|$ is the superficial velocity magnitude. Superficial velocity at any cross section through the porous medium is defined as the volume flow rate divided by the total cross sectional area (i.e. area occupied by both fluid and solid) [19].

A typical channel Reynolds number in an automotive catalyst monolith usually varies between 10 and 1000, so the pressure drop (or flow resistance) is normally prescribed by the Hagen-Poiseuille equation for fully developed laminar flow as in equation 5.

$$\frac{\Delta P}{L} = \frac{(2f\,\mathrm{Re}_c)\mu}{\psi d_h^{\,2}}u \qquad (5)$$

where fRe_c is a constant dependent on the channel cross sectional shape (for unwashcoated ceramic substrate the shape is square hence fRe_c=14.227), μ is the dynamic viscocity, ψ is the substrate porosity, d_h is the channel hydraulic diameter, and u is the channel superficial velocity.

Since the flow in the channel is essentially unidirectional, the permeability coefficients α and β in the radial and circumferential directions are set to large values (10^6) to suppress the momentum transfer in these directions. In the channel axial direction, for square cross section channels α is set to a very small valued (10^{-6}) and β can be subsequently calculated from equations 4 and 5:

$$\beta = \frac{(2f\,\mathrm{Re}_c)\mu}{\psi d_h^2} \qquad (6)$$

As a consequence of flow separation and recirculation within the diffuser the gas impinges on the substrate front face at an oblique angle in certain regions, introducing an additional pressure loss at the channel entry. In a previous study [20] the term $\frac{1}{2}\rho u_r^2$ was used to describe this additional channel pressure loss, where ρ is the gas density and u_r is the flow's radial velocity prior to entering the channel. Hence the porous medium permeability coefficient β is prescribed as in equation 7, when the flow 'entrance effect' is incorporated.

$$\beta = \frac{(2f\,\mathrm{Re}_c)\mu}{\psi d_h^2} + \frac{\frac{1}{2}\rho u_r^2}{Lu} \qquad (7)$$

SIMULATION RESULTS AND COMPARISON WITH MEASURMENTS

PRELIMINARY STUDIES

The PISO algorithm in STAR-CD was used for transient simulations. To facilitate convergence and improve accuracy, every transient simulation was restarted from a previously converged steady flow CFD run, the converged flow field of the steady case providing the initial condition for the transient simulation. Preliminary studies were performed to investigate various parameters that could affect the transient solutions for ~72000 Re and ~98 Hz flow condition.

First, preliminary tests were performed to determine numerical cyclic repeatability, using 200 iterations per cycle (time step = 5.125e-05 s) and 5 cycles in total. Figure 10 shows the results, which include (a) the cycle-averaged velocity profile comparisons in the measurement plane and (b) the instantaneous velocity profile comparisons at the time instant when the inlet velocity is at a peak. The first two cycles have relatively large cycle-to-cycle variation but the third, fourth and fifth cycles show very small differences. Therefore further simulations were conducted for only four complete cycles and the predictions were processed using the data saved in the last cycle.

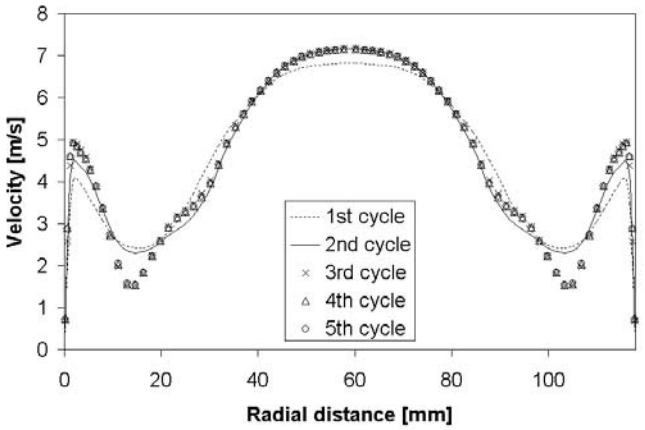

(a) cycle-averaged velocity profile comparisons

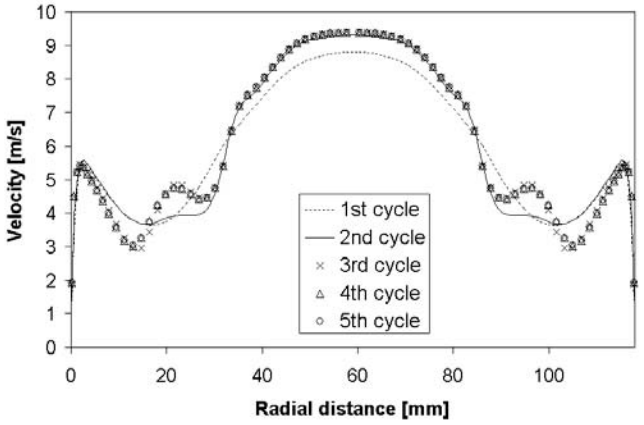

(b) instantaneous velocity profile comparisons when the inlet velocity is at peak

Figure 10 - Cycle-to-cycle variation comparisons

Second, two cases were simulated to determine the time step size for the transient simulations, featuring 200 and 1000 time steps per cycle respectively. Both cases were run for four complete cycles. The time steps were 5.125e-05 s and 1.025e-05 s respectively. Figure 11 compares the two cases for the predicted cycle-averaged profile and instantaneous profile when the inlet velocity is at a peak. It suggests that there is only a small gain in accuracy using 1000 time steps per cycle for the ~98 Hz pulsation. To facilitate post-processing, all the transient CFD simulations in this study used 200 time steps per cycle irrespective of frequency. The lowest frequency in this study was ~15 Hz, giving the largest time step of 3.3333e-4 s. Even for this simulation, the Courant numbers were well below the recommended maximum allowable values (of the order of 100) [19].

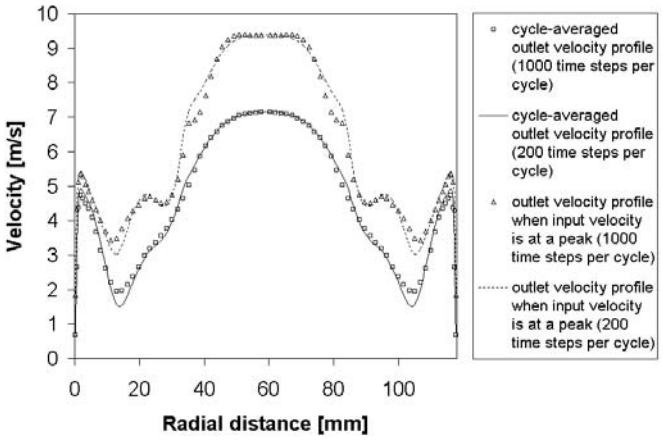

Figure 11 - Comparison of different time step sizes

Finally, four cases were simulated to determine which differencing scheme and porous medium resistance formula correlated best with experiment. The differencing schemes used for momentum and turbulence variables were a second order MARS and a first order UD scheme. Substrate resistance was considered either with or without the 'entrance effect' correction. The predicted cycle-averaged velocity profiles in the measurement plane were compared with measurements for all four cases, as shown in figure 12. Without the 'entrance effect', simulations underpredicted the flow maldistribution. Incorporation of the flow entrance effect improved the prediction of the velocities in the central region of the substrate, where the mass flow rate is high. Figure 12 also shows that the MARS scheme gave predictions of the maximum velocity closer to experiment than the UD scheme. These findings are consistent with a previous steady flow CFD study [20].

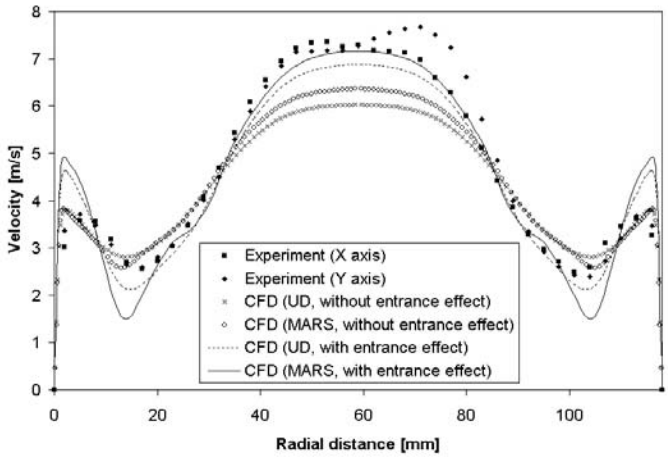

Figure 12 - Comparison of different differencing schemes and substrate flow resistance formulae

In summary, it was decided that for all the transient simulations, MARS was the differencing scheme of choice for the momentum and turbulence variables, porous medium flow resistance was prescribed by the Hagen-Poiseuille equation together with the 'entrance effect', four complete cycles were performed with 200 iterations per cycle, and predictions were extracted from the data saved for the last cycle.

COMPARISONS WITH MEASUREMENTS

Comparisons between CFD and experiments for the inlet pulse shapes used in this study

Cycle-averaged velocity profiles

Figure 13 compares the predicted cycle-averaged outlet velocity profiles with measurements for ~31 Hz pulsation frequency with different mass flow rates. Figure 14 show comparisons between CFD and measurements with ~70000 Re for different pulsation frequencies. In general, fairly good agreement was achieved between the predictions and experiments for the cycle averaged outlet velocity profiles in the central region. The apparent discrepancy at low Re (figure 13 a) is exaggerated due to the velocity scale.

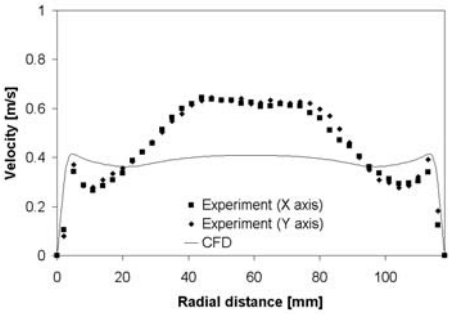

(a) ~7000 Re, ~31 Hz

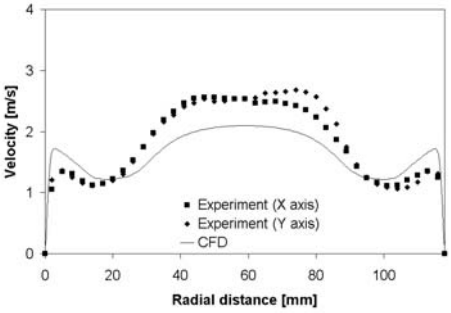

(b) ~29000 Re, ~31 Hz

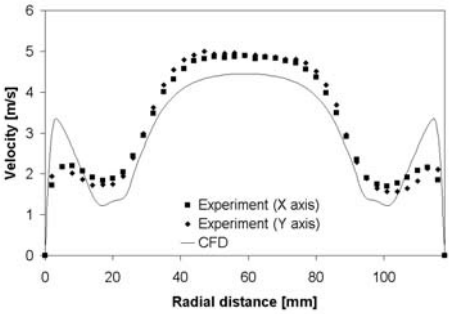

(c) ~48000 Re, ~31 Hz

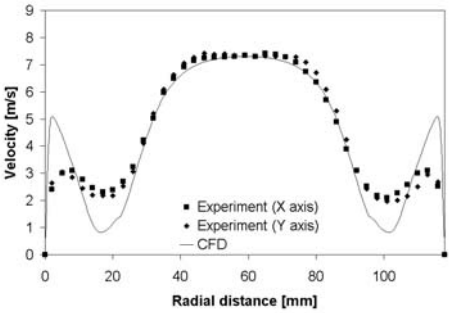

(d) ~67000 Re, ~31 Hz

Figure 13 - Comparisons between CFD and experiment at ~31 Hz for different mass flow rates

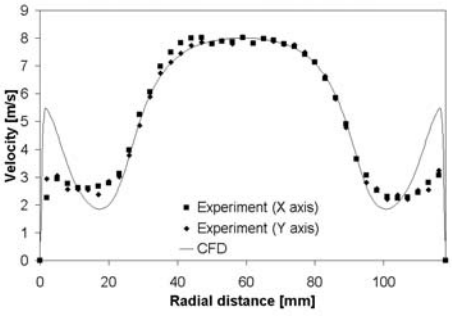

(a) ~73000 Re, steady state

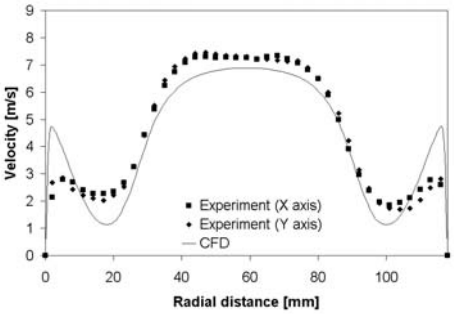

(b) ~65000 Re, ~15 Hz

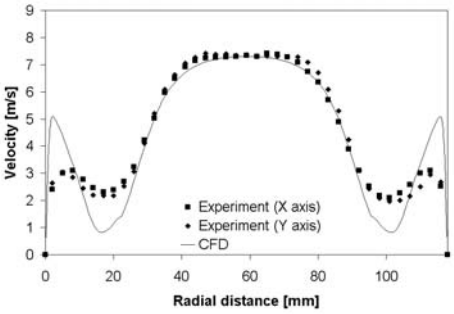

(c) ~67000 Re, ~31 Hz

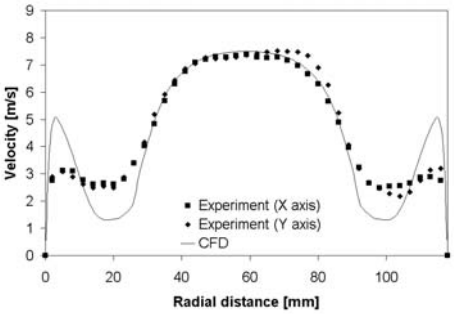

(d) ~70000 Re, ~49 Hz

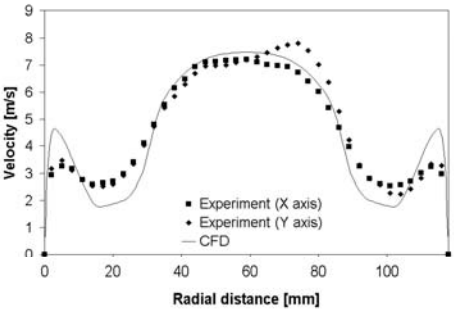

(e) ~70000 Re, ~63 Hz

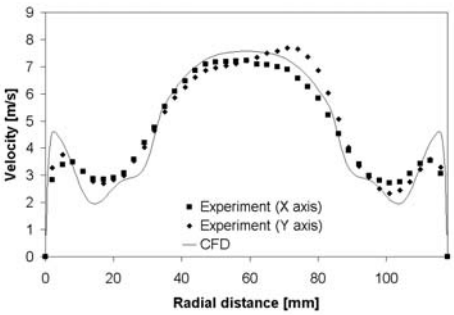

(f) ~72000 Re, ~78 Hz

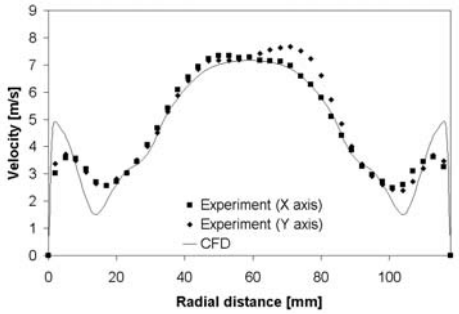

(g) ~72000 Re, ~98 Hz

Figure 14 - Comparisons between CFD and experiment with ~70000 Re for different frequencies

Instantaneous velocity profiles

For further validation, the instantaneous velocity profiles and time history of the velocity at the centre of the measurement plane were compared. Two cases are reported, ~67000 Re, ~31 Hz, and ~72000 Re, ~98 Hz respectively. To capture true instantaneous velocity profiles there would be a need for approximately 50 probes in fixed locations in the measurement plane, which was not feasible. Instead, the velocity traces recorded at each individual traverse location were used. Utilising the timing signal from the pulse generator, the velocity trace at each spatial location was ensemble averaged over a minimum 25 cycles at several time instants within a pulse.

Figure 15 and 16 compare predictions with measurements for the above two flow conditions. In both figures, (a) shows the inlet pulse shape for one cycle for both experiment and CFD, (b) shows the measured instantaneous velocity profiles corresponding to all the selected time instants in (a) and the mean experimental profile, (c) shows the CFD predictions of the instantaneous velocity profiles corresponding to the selected time instants in (a) and the mean CFD profile, (d) - (i) compare predictions with the experimental data at each selected time instant in (a), and finally (j) shows the velocity history comparison between CFD and experiment at the centre of the measurement plane.

Spatial comparisons between CFD and experiment as illustrated by (d) - (i) for both cases showed that predictions in general agreed fairly well with measurements for the central region. The correlation is relatively poor in the outer region. Interestingly for some time instants in both cases when the inlet velocity is low (t = 0.0025 and 0.005 in figure 15, t = 0.0015 in figure 16), CFD predicted some flow reversals in the region ~20 mm from the wall. This possible reverse flow, however, could not be detected in the experiment as the hot wire used in the measurements was a single wire sensor. The ambiguity of the flow reversal with low velocities may contribute to the relatively poor correlation between CFD and measurement for the region ~20 mm from the wall. Nevertheless, for the bulk central region where the mass flow rate is high, the agreement between predictions and measurements was satisfactory.

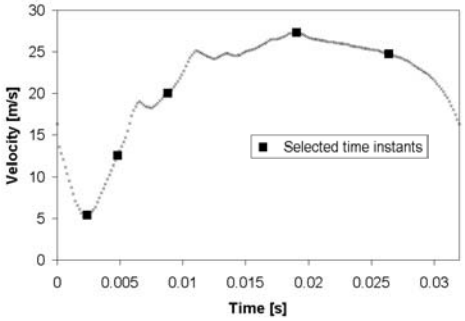

(a) inlet velocity for one cycle (experiment and CFD)

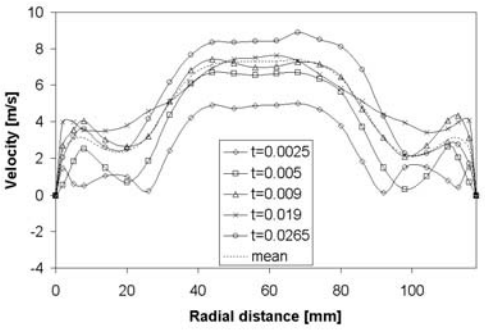

(b) instantaneous and mean velocity profile (experiment only)

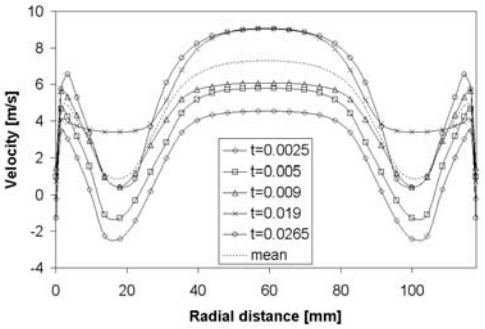

(c) instantaneous and mean profile (CFD predictions only)

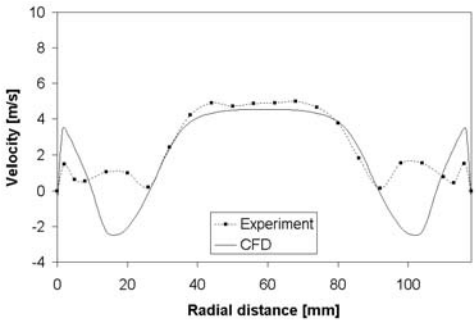

(d) instantaneous velocity profile at t = 0.0025 s (experiment and CFD)

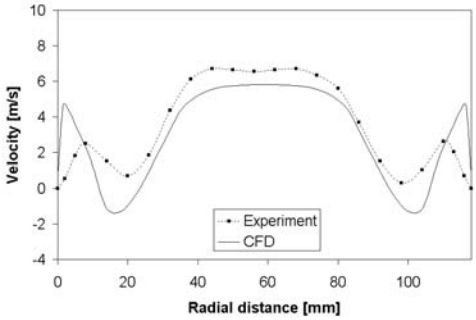

(e) instantaneous velocity profile at t = 0.005 s (experiment and CFD)

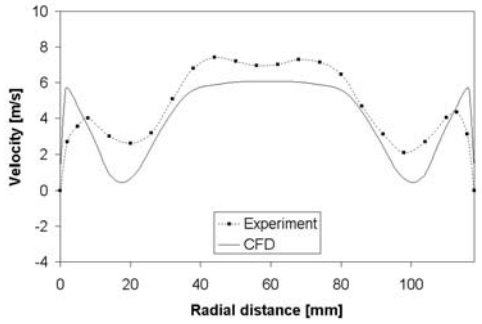

(f) instantaneous velocity profile at t = 0.009 s (experiment and CFD)

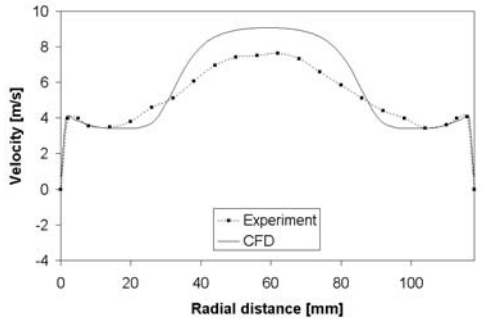

(g) instantaneous velocity profile at t = 0.0019 s (experiment and CFD)

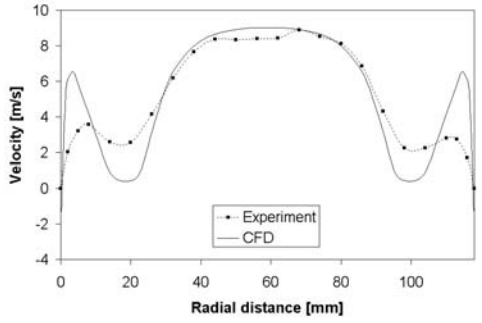

(h) instantaneous velocity profile at t = 0.0265 s (experiment and CFD)

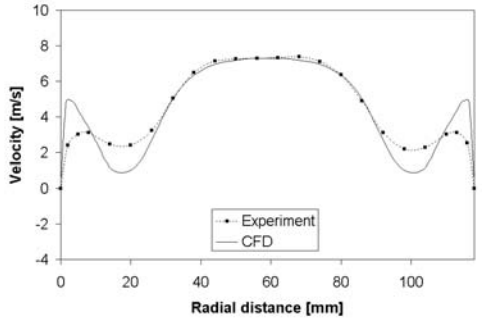

(i) mean velocity profile (experiment and CFD)

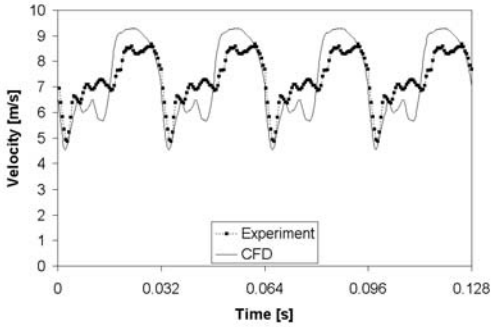

(j) velocity history at the centre of measurement plane (exp. and CFD)

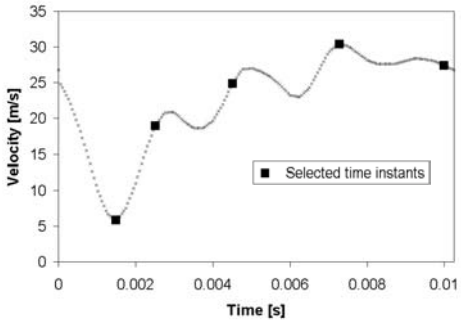

(a) inlet velocity for one cycle (experiment and CFD)

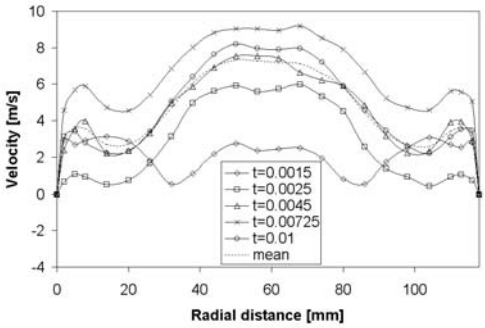

(b) instantaneous and mean velocity profile (experiment only)

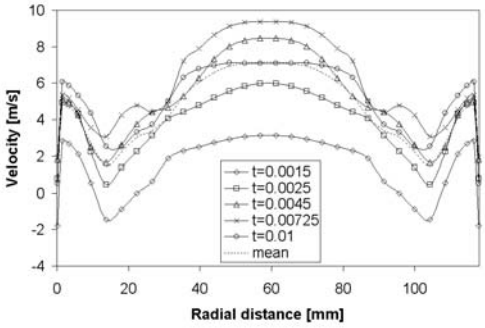

(c) instantaneous and mean profile (CFD predictions only)

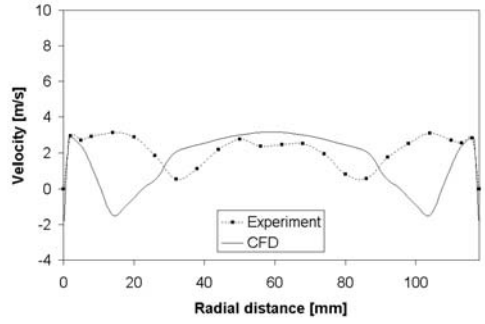

(d) instantaneous velocity profile at t = 0.0015 s (experiment and CFD)

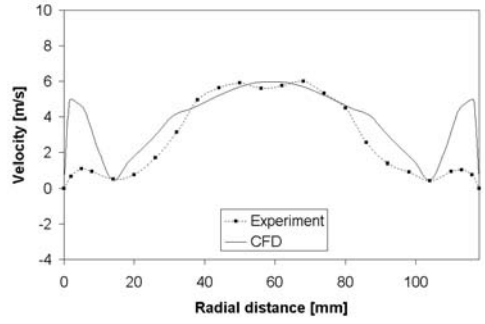

(e) instantaneous velocity profile at t = 0.0025 s (experiment and CFD)

Figure 15 - Comparisons between CFD and experiment (~67000 Re and ~31 Hz)

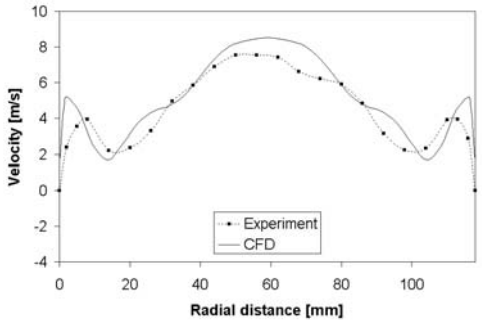

(f) instantaneous velocity profile at t = 0.0045 s (experiment and CFD)

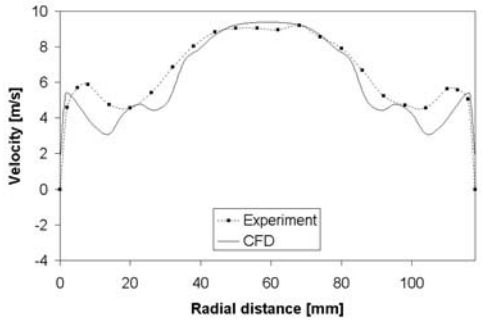

(g) instantaneous velocity profile at t = 0.00725 s (exp. and CFD)

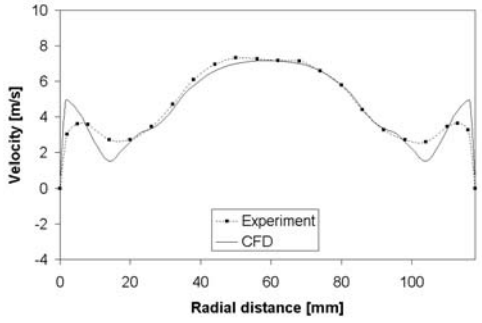

(h) instantaneous velocity profile at t = 0.01 s (experiment and CFD)

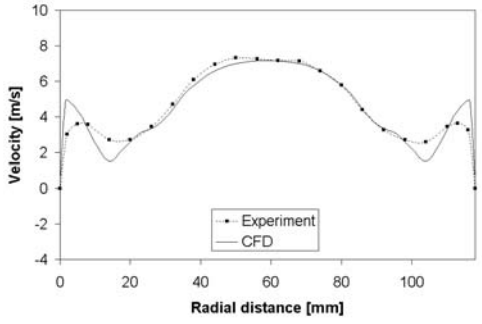

(i) mean velocity profile (experiment and CFD)

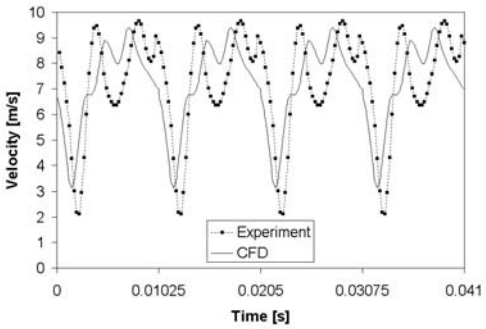

(j) velocity history at the centre of measurement plane (exp. and CFD)

Figure 16 - Comparisons between CFD and experiment (~72000 Re and ~98 Hz)

It is interesting to compare the instantaneous experimental/CFD velocity profiles at the time instant corresponding to the minimum inlet velocity for both cases (figure 15(d) and figure 16(d)). For approximately the same inlet velocities (~5 m/s), the profile in the ~98 Hz case is much flatter than that in the ~31 Hz case. This suggests that at higher frequencies, the flow seems not be able to establish the inertia dominated flow due to insufficient time and/or enhanced flow mixing as discussed earlier. Figure 15(j) and 16(j) show temporal comparisons for the velocity trace at the centre of the measurement plane. Predicted pulse shapes were similar to those measured. This reconfirms that in the central region, CFD agrees well with experiments. For the ~98 Hz case the amplitude of the lowest exit velocity is much lower than that of the ~31 Hz case, probably due to the above-mentioned frequency effect.

Comparisons between CFD and experiments for the inlet pulse shapes used in previous study [21]

Transient simulations were also performed for the inlet pulse shapes used in [21]. Figure 17 shows the comparisons between predictions and measurements. Simulations did not agree well with measurements. Since the same computational mesh, temporal and spatial differencing schemes, time step size and porous medium flow resistance formula were used for simulations with inlet pulse shapes generated in both studies, the relatively poor prediction shown in figure 17 was thought to be probably attributed to the inaccuracy of the turbulence model used. The RANS k-ε model was originally derived for steady flow conditions. For periodic flows ensemble averaging is formally used and the turbulence viscosity concept is assumed to apply, using ensemble derived statistics for turbulent kinetic energy k and its dissipation rate ε. The justification for this approach is far from clear. The relatively poor predictions under strongly pulsating flows may reflect the inadequacies of this approach for conditions far removed from steady flow. It suggests that under such conditions alternative treatments may be necessary. One such possibility is Large Eddy Simulation (LES). This relatively new approach may offer the prospect of improving predictive capability for strongly pulsating flows.

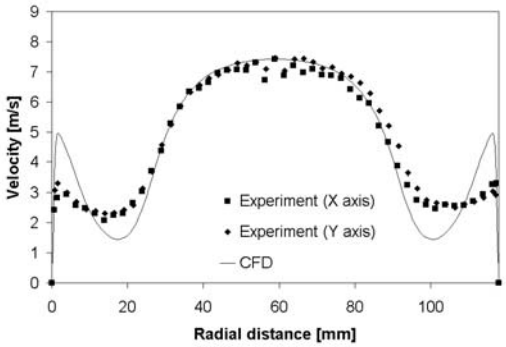

~72000 Re, steady state

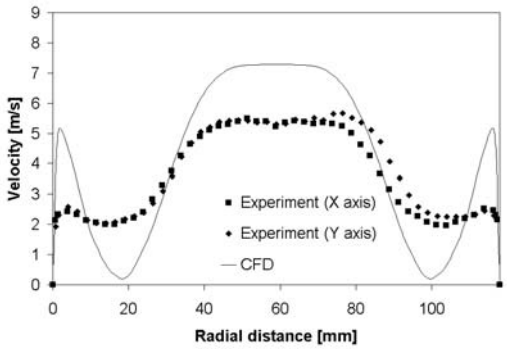

~57000 Re, ~17 Hz

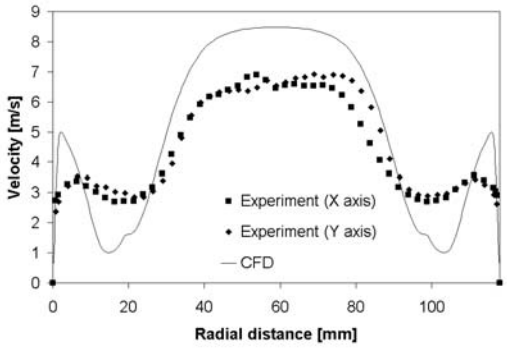

~72000 Re, ~31 Hz

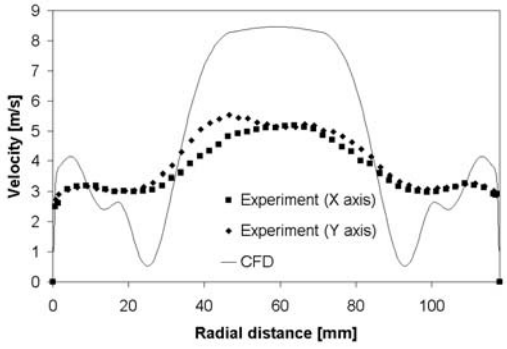

~ 66000 Re, ~63 Hz

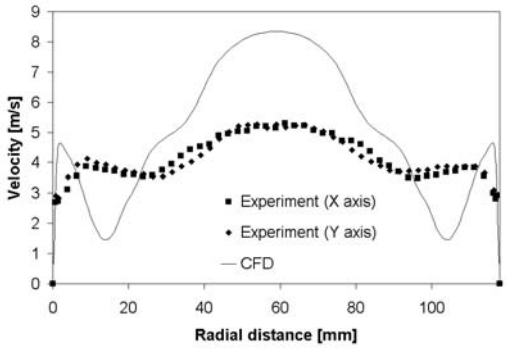

~73000 Re, ~100 Hz

Figure 17 - Comparisons between CFD and experiments for inlet pulse shapes used in reference [21]

CONCLUSION

The effect of mass flow rate and pulsation frequency on the flow distribution across the monolith of an axisymmetric catalyst assembly has been studied. Lower mass flow rate and higher frequency in general caused more uniformly distributed flow. Experimental results at high Reynolds number were compared between two studies using different inlet pulse shapes. The degree of flow maldistribution was largely influenced by the inlet velocity pulse shapes. For the inlet pulse with higher peak/mean ratio, the flow is less maldistributed at all frequencies.

Less maldistributed flow across the monolith makes the catalyst utilisation and conversion efficiency more spatially uniform, leading to better catalyst performance and longer life times. This flow rig study suggests that for production systems, the flow maldistribution will depend on mass flow rate (engine load), pulsation frequency (engine speed) and pulse shapes (load, speed and engine configuration). The net effect of these parameters on flow distribution needs to be evaluated on running engines, which will form the basis of a follow-up research programme.

Transient CFD simulations, using the second order MARS differencing scheme and incorporating the flow entrance effect, agreed fairly well with measurements in the bulk central region of the monolith for relatively gentle pulsating flow conditions. For more severely pulsating flows, the current CFD model performed less satisfactorily. It suggests that the RANS k-ε turbulence modelling approach is not applicable under such conditions.

ACKNOWLEDGEMENT

The authors would like to acknowledge the support from ArvinMeritor Inc.

REFERENCES

1. Howitt, J. S. and Sekella, T. C., *Flow Effects in Monolithic Honeycomb Automotive Catalytic Converters*, SAE paper 740244, 1974.
2. Comfort E. H., *Monolithic catalytic converter performance as a function of flow distribution*, ASME Winter Annual Meeting, Paper No. 74-WA/HT-30, 1974
3. Martin, A. P., Will, N. S., Bordet, A., Cornet, P., Gondoin, C. and Mouton, X., *Effect of Flow Distribution on Emissions Performance of Catalytic Converters*, SAE paper 980936, 1998
4. Benjamin, S. F., Clarkson, R. J., Haimad, N., Girgis N. S., *An Experimental and Predictive Study of the Flow Field in Axisymmetric Automotive Exhaust Catalyst Systems*, SAE Transactions, vol 105, Journal of Fuels and Lubricants, Section 4, pp 1008-1019
5. Lai, M. C., Kim, J. Y., Cheng, C. Y., Li, P., Chui, G. and Pakko, J. D., *Three-Dimensional Simulations of Automotive Catalytic Converter Internal Flow*, SAE paper 915200, 1991
6. Weltens, H., Bressler, H., Terres, F., Neumaier H. and Rammoser D., *Optimisation of Catalytic Converter Gas Flow Distribution by CFD Prediction*, SAE paper 930780, 1993

7. Arias-Garcia, A., Benjamin, S. F., Zhao, H. and Farr, S., *A comparison of Steady, Pulsating Flow Measurements and CFD Simulations in Close Coupled Catalysts*, SAE paper 01FL-335, 2001
8. Zhao, F. Q., Bai, L., Liu, Y., Chue, T. H. and Lai, M. C., *Transient Flow Characteristics Inside the Catalytic Converter of a Firing Gasoline Engine*, SAE paper 971014, 1997
9. BAI, L., ZHAO, F. Q., Liu, Y. and Lai, M. C., *Transient Flow and Pressure Characteristics inside a Closed-Coupled Catalyst Converter*, SAE paper 982548, 1998
10. Park, S. B., Kim, H. S., Cho, K. M. and Kim, W. T., *An Experiemtanl and Computational Study of Flow Characteritics in Exhaust Manifold and CCC (Close-Coupled Catalyst),* SAE paper 980128, 1998
11. Payri, F., Benajes, J. and Galindo, J., *One-Dimensional Fluid-Dynamic Model for Catalytic Converters in Automotive Engines*, SAE paper 950785, 1995
12. Bressler, H., Rammoser, D., Neumaier, H. and Terres, F., *Experimental and Predictive Investigation of a Close Coupled Catalytic Converter with Pulsating Flow*, SAE paper 960564, 1996
13. Cho, Y. S., Kim, D. S., Han, M., Joo, Y., Lee, J. H. and Min, K. D., *Flow Distribution in a Close Coupled Catalytic Converter,* SAE paper 982552, 1998
14. Liu, Z., Benjamin, S. F., Roberts, C. A., Zhao, H. and Arias-Garcia, A*., A Coupled 1D/3D Simulation for the Flow Behaviour inside a Close-Coupled Catalytic Converter*, 2003 SAE/JSAE Spring Fuels & Lubricants Meeting, Japan May 2003, JSAE paper No 20030045, SAE paper No 2003-01-1875
15. Bella, G., Rocco, V. and Maggiore, M., *A Study of Inlet Flow Distortion Effects on Automotive Catalytic Converters*, Journal of Engineering for Gas Turbines and Power, July 1991, Vol. 113/419
16. Jeong, S. and Kim Taehun, CFD Investigation of the 3-Dimensional Unsteady Flow in the Catalytic Converter, SAE paper 971025, 1997
17. Jeong, S. J. and Kim, W. S., *A Three-dimensional Numerical Study of the Effect of Pulsating Flow on Conversion Efficiency Inside a Catalytic Converter,* Proc. Instn. Mech. Engrs. Vol. 215 Part D, 2001
18. Benjamin, S. F., Roberts, C. A. and Wollin, J., *A Study of the Effect of Flow Pulsations on the Flow Distribution within Ceramic Contoured Catalyst Substrates*, SAE 2001-01-1996, 2001 SAE Spring Fuels and Lubricants conference in Orlando, Florida, USA, 2001
19. Computational Dynamics Ltd, *STAR-CD Users Guide (version 3.15),* 2001
20. Benjamin, S. F., Haimad, N., Roberts, C. A. and Wollin J. *Modelling the Flow Distribution Through Automotive Catalytic Converters,* Proc. Instn. Mech. Engrs. Vol. 215 Part C, 2001
21. Benjamin, S. F., Roberts, C. A., Wollin, J., *A Study of Pulsating Flow in Automotive Catalyst Systems*, Exp. in Fluids (2002) 33: 629-639, DOI: 10.1007/s00348-002-0481-0, 2002
22. Wollin, J., *A study of Pulsating Flow in Automotive Exhaust Catalyst Systems,* Ph.D thesis, Coventry University, 2001

CONTACT

Prof S. F. Benjamin
Coventry University
School of Engineering
Priory Street, Coventry
CV1 5FB, United Kingdom
Email: s.benjamin@coventry.ac.uk

NOMENCLATURE AND ACRONYMS

d_h	Channel hydraulic diameter
fRe_c	Constant
k	Turbulent kinetic energy
L	Substrate channel length
$\dot{m}$	Mass flow rate
Δp	Pressure loss
Re	Reynolds number
S	Cross sectional area of the monolith
u	Superficial velocity
u_r	Radial velocity of gas prior to entering substrate channel
$\overline{V}$	Mean velocity across the monolith
V_i	Individual channel velocity
$\lvert \boldsymbol{v} \rvert$	Superficial velocity magnitude
x,y,z	Cartesian coordinate system in the flow rig
X,Y,Z	Cylindrical coordinate system in the CFD mesh
α, β	Permeability coefficients
ε	Turbulent kinetic energy dissipation rate
μ	Dynamic viscosity
ρ	Density
σ_V	Variation of the velocity
Λ	Non-uniformity index
Ψ	Substrate porosity

CCC	Close Coupled Catalyst
CFD	Computational Fluid Dynamics
CPSI	Cells Per Square Inch
HWA	Hot Wire Anemometry
LES	Large Eddy Simulation
RANS	Reynolds Averaged Navier Stokes equation
UBC	Under Body Catalyst